Optics & Laser Technology 145 (2022) 107482

Contents lists available at ScienceDirect

Optics and Laser Technology

journal homepage: www.elsevier.com/locate/optlastec

Ternary 2D $Mo_{(1-x)}W_xS_2$ as a saturable absorber for femtosecond mode-locked all fiber lasers

Jingjing Lei [a], Junli Wang [a,*], Xiaoli Wang [a], Zhiyi Wei [b]

[a] School of Physics and Optoelectronic Engineering, Xidian University, Xi'an 710071, China
[b] Beijing National Laboratory for Condensed Matter Physics, Institute of Physics, Chinese Academy of Sciences, Beijing 100190, China

ARTICLE INFO

Keywords:
Ternary two-dimensional material
Er-doped fiber lasers
Mode-locked fiber lasers

ABSTRACT

In this paper, we utilized the ternary $Mo_{(1-x)}W_xS_2$ alloys to fabricate $Mo_{0.5}W_{0.5}S_2$ film, which serve as a ultrashort pulse mode-locker in erbium-doped all fiber lasers (EDFL). The modulation depth, saturable intensity and unsaturated loss of the film SA were 12%, 4.5 MW/cm^2 and 67.1% respectively. Stable self-mode-locking pulses could be achieved with a threshold pump power of 60 mW. With the increasing pump power, the pulse was centered at 1556.8 nm ~ 1558.1 nm with pulse width of 575 fs ~ 800 fs. The shortest pulse width, fundamental repetition rate and maximum pulse energy is 575 fs, 4.873 MHz, and 0.154 nJ, respectively. The signal to noise ratio (SNR) was measured to be about 53 dB. For the first time, we have experimentally demonstrated a mode-locked EDFL based on $Mo_{0.5}W_{0.5}S_2$ SA. To the best of our knowledge, this was the first realization of femtosecond photonics based on $Mo_{0.5}W_{0.5}S_2$ SAs. Our results suggest that $Mo_{0.5}W_{0.5}S_2$ SA is a promising candidate for mode-locked ultrafast fiber laser in optoelectronic and optical communications applications.

1. Introduction

In recent years, ultrafast fiber lasers have attracted significant attention in applications include nonlinear optics, medical surgery, and precise optical metrology and remote sensing technology [1–3]. Two-dimensional (2D) materials have unique optoelectronic properties comparing with many traditional materials, especially their outstanding nonlinear optical characteristics, which have shown great potential in building high-performance and new functional optoelectronic devices. In the researches and applications of 2D materials, it is one of the most important research directions to use them as SAs for laser pulse generation and modulation. Different kinds of SAs are widely used in mode-locked fiber lasers, such as single wall carbon nanotubes (SWCNT) [4], graphene, transition metal dichalcogenides (TMDs) (MoS_2, ReS_2, WS_2, WSe_2, $MoTe_2$, etc.) [5–9], black phosphorus (BP) [10], topologic insulators (TIs) [11], MXene [12], and Graphene [13]. These 2D SAs based fiber lasers have compact structures with stable and high beam quality output. More importantly, the structures can obtain desired bandgaps by adjusting the layer number of materials. The reported bandgaps of bulk and double-layer MoS_2 are 1.29 eV and 1.75 eV, respectively. The corresponding bandgaps of WS_2 are about 1.31 eV and 1.57 eV, respectively [14]. Compared with the many binary TMDs, a composition-dependent band gap emission of $Mo_{(1-x)}W_xS_2$ alloys, provides more freedom to regulate its energy bandgap by altering the proportion of two elements (Mo and W). Photoluminescence characterization has shown tunable band gap emission continuously tuned from 1.82 eV (reached at x = 0.20) to 1.99 eV (reached at x = 1) [15]. Similar to other TMD materials, the transition metal (M) atoms (M: such as Mo, W, Re) are covalently bounded to the chalcogen atoms (X: such as S, Se) and the MX_2 layers are connected by van der Waals forces. In comparison with other ternary 2D SA, such as $ReS_{2(1-x)}Se_{2x}$[16], $Ti_3C_2T_x$[17], and Ta_2NiS_5[18], $Mo_{0.5}W_{0.5}S_2$ SA based can obtain the shorter pulse width in 1.5 μm spectral regions.

Passively Q-switching based on $Mo_{(1-x)}W_xS_2$ alloys were achieved at 1 μm, 1.3 μm, 1.5 μm, 1.6 μm, and 2 μm, respectively [19–23], which showed broadband saturable absorption characteristics of ternary $Mo_{(1-x)}W_xS_2$ alloys. But the mode locked laser pulse could not be obtained only by changing loss and gain in the ring cavity. One possible reason could be the low density of SA in the cavity. The home-made films normally have uneven surface and uncontrollable thickness, which make it difficult to attach effectively to the end face of the fiber. As a result, the effective interaction areas are reduced, which decreases the density of SA in the cavity. On the other hand, the dispersion and nonlinear effects also need to be optimized. In order to realize mode-

* Corresponding author.
E-mail address: dispersion@126.com (J. Wang).

https://doi.org/10.1016/j.optlastec.2021.107482
Received 19 October 2020; Received in revised form 20 July 2021; Accepted 23 August 2021
Available online 9 September 2021
0030-3992/© 2021 Elsevier Ltd. All rights reserved.

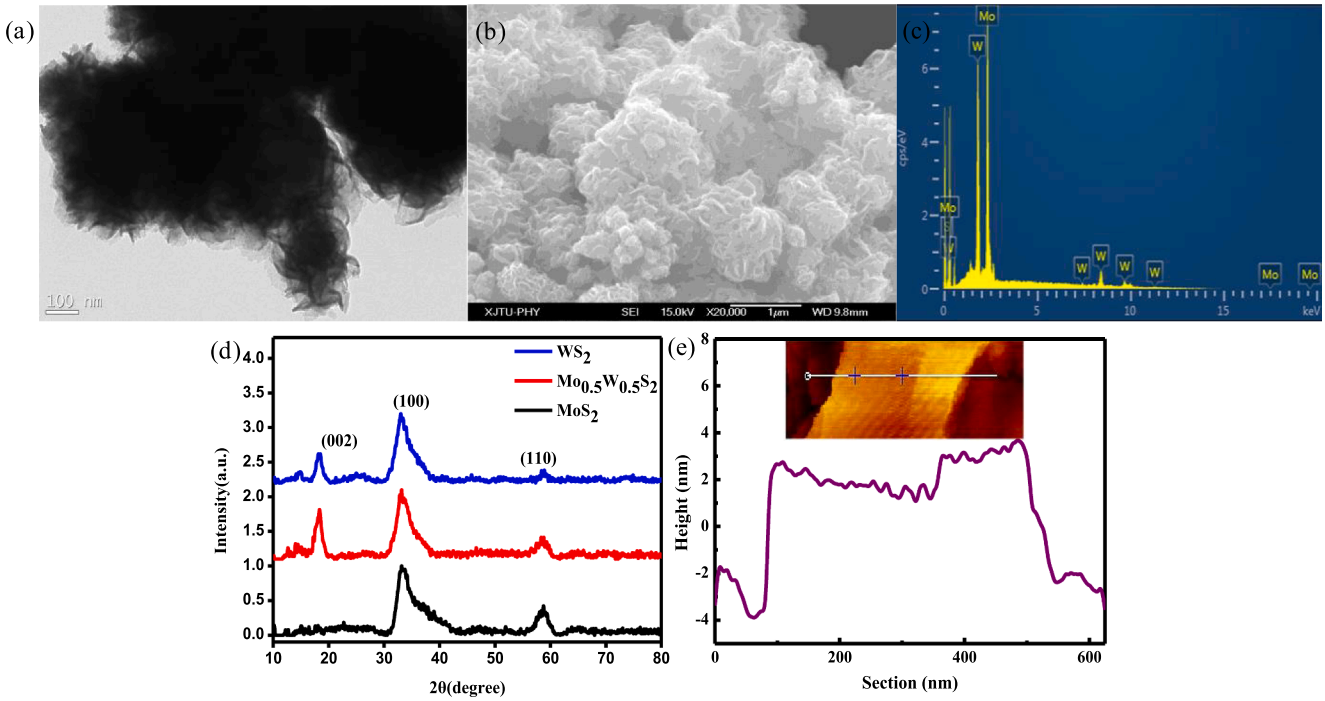

Fig. 1. (a) TEM image with 100 nm scale. (b) SEM image with 1 μm scale. (c) Energy Dispersive x-ray spectroscopy of the $Mo_{0.5}W_{0.5}S_2$ nanosheet [24]. (d) The X-ray diffraction (XRD) pattern of WS_2, $Mo_{0.5}W_{0.5}S_2$, MoS_2. (e) AFM image of $Mo_{0.5}W_{0.5}S_2$ nanosheet.

locking at 1.5 μm, two measures were taken in this experiment. The first was the improvement of SA/PVA film transfer technology. We found that by applying suitable amount of alcohol on the end face of the fiber, the SA/PVA film then could be tightly attached to the end face of the fiber. The second measure was increasing the negative dispersion to balance the nonlinear effect in the cavity. Through the above improvements, we experimentally demonstrated, for the first time ever to the best of our knowledge, an Er-doped fiber laser (EDFL) based on $Mo_{0.5}W_{0.5}S_2$ film via microwave-assisted solvothermal method (MAST). The nonlinear absorption characteristics of $Mo_{0.5}W_{0.5}S_2$ were measured by twin detector technique. A modulation depth of 12% and saturating intensity of 4.5 MW/cm^2 were measured. By sandwiching the $Mo_{0.5}W_{0.5}S_2$/PVA films between the two fiber end faces, we successfully obtained a stable mode locked pulse of 575 fs and a spectral bandwidth of 6.33 nm at 1.56 μm.

2. Material preparation and characterization

The $Mo_{(1-x)}W_xS_2$ alloys were synthesised by MAST [24]. The transmission electron microscope (TEM) image of $Mo_{0.5}W_{0.5}S_2$ nanosheet structure was showed in Fig. 1(a). The TEM image scale is about 100 nm. The darker area represents the thicker nanomaterial, so high quality few layer nanosheets could be observed at the edge of the cluster. The scanning electron microscope (SEM) was showed in Fig. 1(b). Under the acceleration voltage of 15 kV, the magnification of 20000×, the scanning scale of 1 μm, it was obviously that $Mo_{0.5}W_{0.5}S_2$ nanosheets were composed of clusters of nanoflowers with a diameter in the range of 400 nm-800 nm. Fig. 1(c) showed the element composition analysis of $Mo_{0.5}W_{0.5}S_2$ nanosheets with an energy dispersive spectroscopy (EDS). The sample contains S, Mo and W elements, the atomic ratio of which is 62.27:18.08:19.65. Then we characterized and compared the WS_2, $Mo_{0.5}W_{0.5}S_2$, and MoS_2 with the X-ray diffraction method. Fig. 1 (d) showed that the $Mo_{(1-x)}W_xS_2$(x = 1, 0.5 , 0) alloys have three broad diffraction peaks at around 2θ = 14.7°, 33.1°, 58.8°, corresponding to the (002) , (100) , and (110) planes of the hexagonal $Mo_{(1-x)}W_xS_2$, respectively. The result indicated the deficient crystalline in the sample, which could be attributed to the limitation of the MAST method.

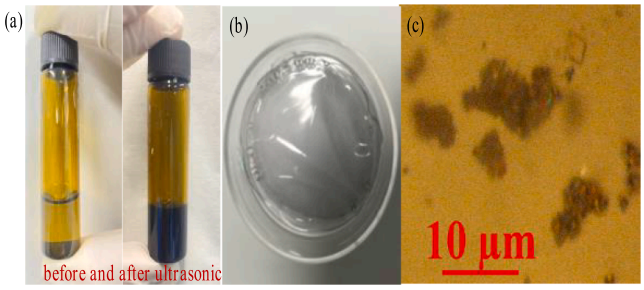

Fig. 2. (a) The image of the $Mo_{0.5}W_{0.5}S_2$/PVA solution before and after sonication.. (b) The transparent $Mo_{0.5}W_{0.5}S_2$/PVA film. (c) Optical microscope image of $Mo_{0.5}W_{0.5}S_2$/PVA film.

Fig. 1(e) was the atomic force microscopy (AFM) image of the $Mo_{0.5}W_{0.5}S_2$ nanosheet, which showed that the size of the $Mo_{0.5}W_{0.5}S_2$ nanosheet is about 400 nm and the thickness is close to 8 nm.

The most common transmission coupling sandwiches SA materials between two fiber ends directly. Few layer nanosheet materials embedded in thin organic polyvinyl alcohol (PVA) could be sandwiched too. In order to prepare the $Mo_{0.5}W_{0.5}S_2$/PVA film, we first dissolved 25 mg of $Mo_{0.5}W_{0.5}S_2$ powder into 20 mL of Polyvinyl Alcohol solvent, and then obtained $Mo_{0.5}W_{0.5}S_2$/PVA solution after 3 h of stirring and ultrasonic treatment as showed in Fig. 2(a), it can be clearly seen that the $Mo_{0.5}W_{0.5}S_2$/PVA solution was maded a well dispersion of nanomaterial. Then the mixture was dropping onto a culture dish and evaporating in a vacuum drying oven for 12 h. The transparent $Mo_{0.5}W_{0.5}S_2$/PVA film was shown in Fig. 2(b). Fig. 2(c) showed the surface of $Mo_{0.5}W_{0.5}S_2$/PVA film observed under an optical microscope.

For a two-dimensional material with a certain band gap width, its Dirac cone structures are separated by a certain interval between neighboring cones. Only the photon with energy larger than the band gap (ΔE) could excite electrons from the valence band to the conduction band. Under weak light irradiation, the electrons in the valence band continuously absorb photons and are excited to the conduction band

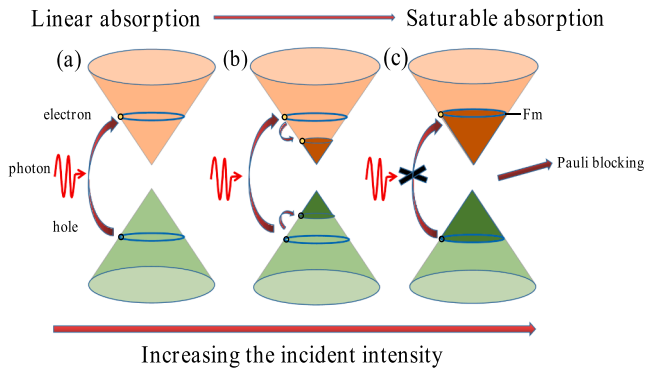

Fig. 3. The image of two-dimensional material nonlinear absorption process.

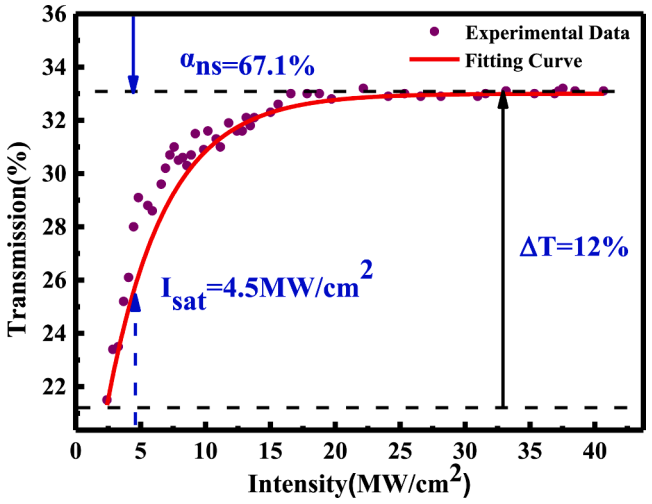

Fig. 4. The nonlinear absorption of $Mo_{0.5}W_{0.5}S_2$/PVA film.

(Light-induced electronic transition process is showed in Fig. 3(a)). The energy state distribution of each electron followed the Fermi-Dirac distribution. With the increasing of light intensity, the carriers gradually reach thermal equilibrium (carriers thermal equilibrium showed in Fig. 3(b)). Before equilibrium, the $Mo_{0.5}W_{0.5}S_2$ SA linearly absorbs the incident photons. However, when the excitation is sufficiently strong, the conduction band and valence band are completely filled by electrons and holes. At this time, the $Mo_{0.5}W_{0.5}S_2$ SA no longer absorbs the incident photons due to the Pauli blocking principle (as shown in Fig. 3(c)), the absorption of photons inside the saturable absorber at a transition energy ceases owing to the band filling. This is the saturable absorption process [25,26]. Generally, when the energy of the single input photon is less than the band gap energy of the SA, the two-photon absorption in the SA easily was triggered by the nonlinear absorption in the help of the enough intensity electrical density of the input laser pulse [27,28]. In this work, few-layer $Mo_{0.5}W_{0.5}S_2$, The bandgap theoretically should be between 0.83 eV and 1.8 eV, the photon energy of the pulsed laser with 1.5 μm wavelength is about 0.83 eV. Two-photon absorption can be achieved to complete the energy transition from the valence band to the conduction band in the SA.

The nonlinear absorption property of the $Mo_{0.5}W_{0.5}S_2$ SA was showed in Fig. 4, which was obtained by using the twin-detector technique. The pump source was a homemade mode-locked fiber laser with a repetition of 44.47 MHz, pulse duration of 900 fs, and center wavelength of 1565 nm, where the output was linked with a 50:50 coupler. One half of the power was measured for reference, and the rest of power was incorporated in the SA. The experimental data and fitting curve of the SA is described by the following formula.

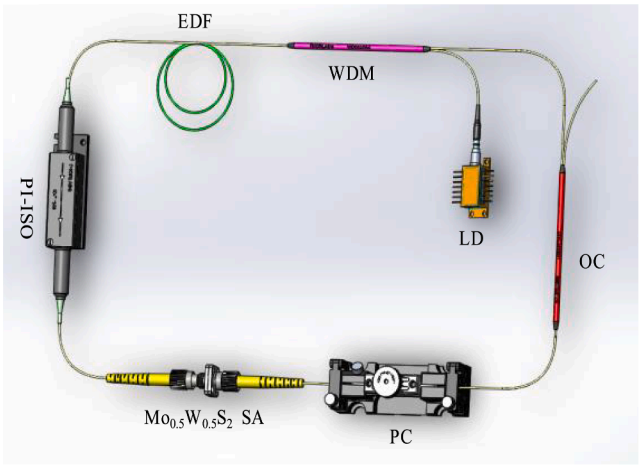

Fig. 5. The Diagram of the mode-locking fiber laser based on $Mo_{0.5}W_{0.5}S_2$ SA.

$$T = 1 - \Delta T \times \exp\left(-\frac{I}{I_{sat}}\right) - A_{ns}$$

Where ΔT is the modulation depth, I is the intensity of laser, T is the transmittance, I_{sat} is the saturation intensity and A_{ns} was the non-saturable absorbance. The I_{sat}, A_{ns}, ΔT of $Mo_{0.5}W_{0.5}S_2$ were 4.5 MW/cm^2, 67.1%, and 12% respectively.

3. Schematic of passively mode-locked fiber lasers

The schematic diagram of $Mo_{0.5}W_{0.5}S_2$ SA based Er -doped all fiber laser (EDFL) was shown in Fig. 5. A 976 nm laser diode (LD) with a maximum output power of 600mW was the pump source. A 980/1550 wavelength division multiplexer (WDM) was connected to LD. A 38 cm highly doped Er fiber (Liekki Er-110–4-125) was the laser gain medium with a dispersion parameter of 12 ps^2/km. The output rate of the optical coupler (OC) was 10%. $Mo_{0.5}W_{0.5}S_2$ SA was sandwiched into two fiber end faces. A polarization controller was used to change the polarization state in the ring cavity. Other fibers and pigtails of the components were single mode fiber-28 (SMF-28). In the cavity, the group velocity dispersions (GVD) of the SMF-28 was −21 ps^2/km, and the total length of the cavity was 41.1 m. Thus, there was a large negative dispersion of −0.84 ps^2 in the cavity.The output was connected to a real-time oscilloscope (Tektronix DPO3053, 500 MHz, 2.5 GS/S, Shanghai, China), an optical spectrum analyzer (HORIBA IHR550, Shanghai, China) with a resolution of 0.05 nm, an commercial autocorrelator (APE Pulse Check USB, Berlin, Germany) and a RF spectrum analyzer (Agilent E4407B, CA, USA).

4. Experimental results and discussion

The self-starting mode-locking operation was observed when the pump power increased to 60 mW by adjusting PC. The repetition rate was 4.873 MHz, corresponding to the length of the cavity. Fig. 6(a) shows the oscilloscope trace of mode-locked pulse trains when pump power was 190mW. The interval between adjacent pulses was 0.205 μs. Fig. 6(b) shows the radio frequency spectra of the output pulse train.

The SNR was 53 dB . The inset shows the 250-MHz span RF spectrum. Fig. 6(c) shows the measured spectrum at different pump power. It possessed the center wavelength of 1558.1 nm, 1557.3 nm, and 1556.8 nm with a bandwidth of 4.18 nm, 5.74 nm, and 6.33 nm when pump power was 190mW, 240mW, and 350mW, respectively. Fig. 6(d) shows the autocorrelation trace of the output pulse and the fitting curve with the sech^2 function at different pump power. It could be clearly observed that mode locking pulse duration decreased significantly with increasing pump power. It had a real pulse width of 800 fs, 647 fs, and 575 fs

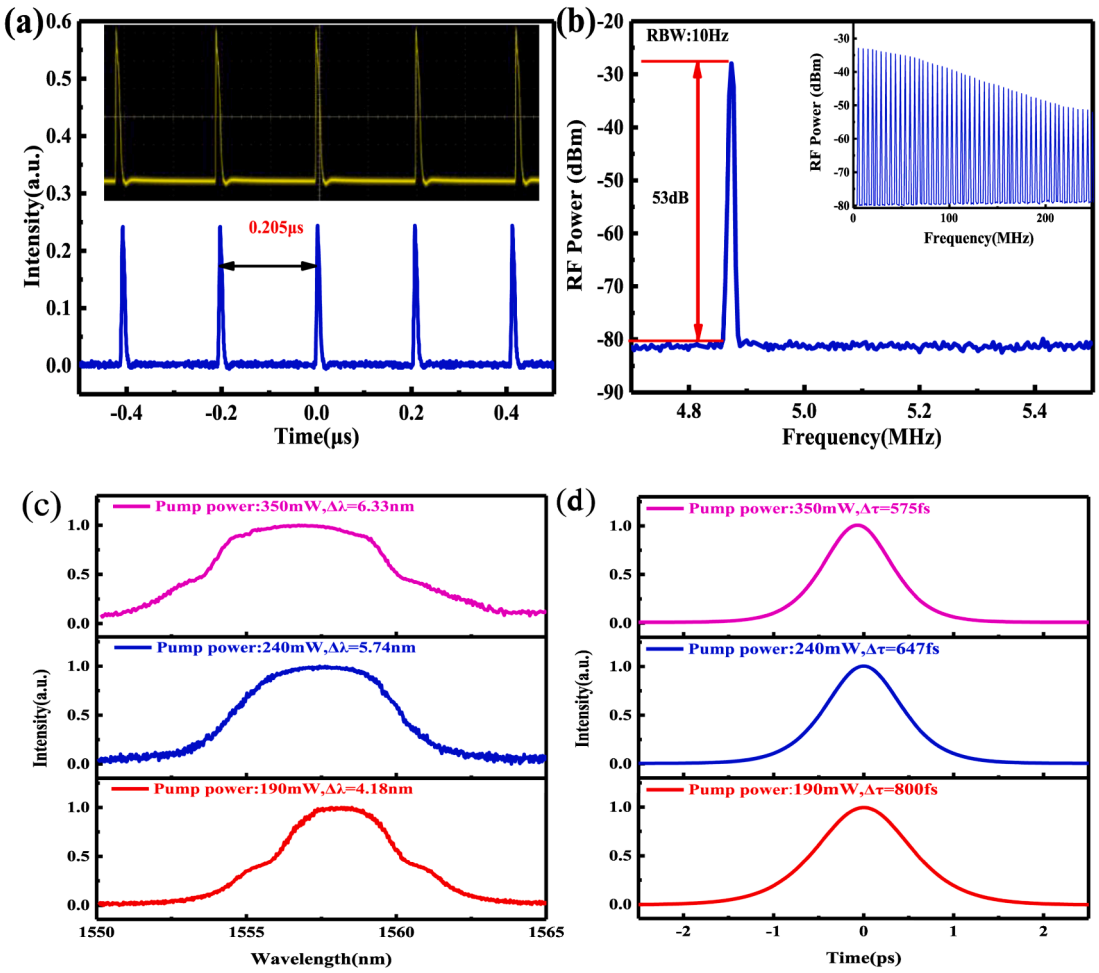

Fig. 6. (a) Pulse trains. Inset: oscilloscope trace; (b) RF spectrum. Inset: is the RF spectrum of 250 MHz span. (c) Optical spectrum at different pump power. (d) Autocorrelation trace at different pump power.

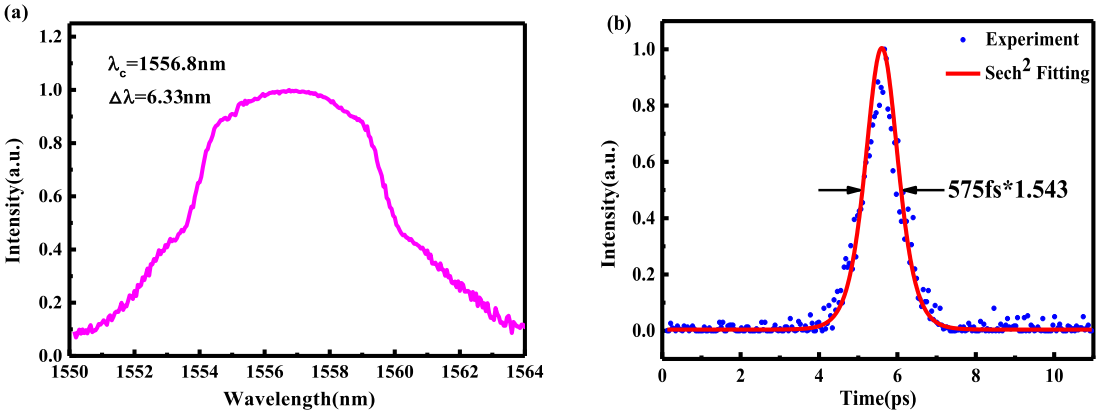

Fig. 7. (a) Optical spectrum at pump power of 350mW. (b) Autocorrelation trace at pump power of 350mW.

respectively. With pump power increasing, the non-linear effect in the laser cavity cancels out the negative dispersion, and the self-phase modulation (SPM) in the cavity broadens the laser pulse spectrum, which can support shorter optical pulses generation. At the same time, the center wavelength of the laser pulse spectrum shifts to the short wavelength direction, and it also exhibits the characteristics of tunable wavelength. Fig. 7(a) shows the widest 3 dB bandwidth was 6.33 nm at a center wavelength of 1556.8 nm. Therefore, the shortest pulse width was 575 fs when pump power was increased to 350mW, as shown in Fig. 7(b). The time-bandwidth product is 0.4498, indicating that the mode-locked pulse was slightly chirped. The maximum output power was only 0.75 mW, corresponding to a single pulse energy of 0.154 nJ. Once the pump power is beyond 350 mW, multi-pulse operation is observed from the oscilloscope. The insertion loss of the material has been measured several times and averaged, and a result of 3.1 dB can be obtained. In addition, according to the nonlinear absorption curve of $Mo_{0.5}W_{0.5}S_2$ SA, the unsaturated loss is 67.1%, which includes the scattering loss caused by surface roughness, absorption loss of defects

Table1
Comparison of this work with other work using different TMDs in Er-doped fiber laser.

SAs	Repetition rate(MHz)	Pulse Width (fs)	Output power (mW)	Pulse energy (nJ)	Peak power (W)	Modulation depth (%)	Refs
MoS_2	12.09	710	1.78	0.147	207	4.3	[29]
Sb_2Te_3	4.75	1800	0.5	0.105	58	–	[30]
MoS_2	29.5	790	4.13	0.14	166	–	[31]
WTe_2	13.98	770	0.04	0.003	3.7	2.85	[32]
$MoSe_2$	5.03	1090	–	–	–	1.4	[33]
$CoSb_3$	22.26	833	0.1	0.004	6.15	5	[34]
$ReS_{2(1-x)}Se_{2x}$	2.95	888	0.812	0.275	310	1.8	[16]
$Ti_3C_2T_x$	8.24	946	1.3	0.158	167	41	[17]
Ta_2NiS_5	2.92	1450	18.6	6.37	4390	11.95	[18]
PdS_2	12.1	803	0.55	0.045	57	1.7	[35]
VSe_2	2.081	1.8 ns	53.21	25.57	14	1.849	[36]
Bi_2Te_3	–	403	–	–	–	27	[37]
n-Bi_2Te_3	–	400	–	–	–	–	[25]
Graphite	7	482	–	–	–	20	[26]
Graphene	–	650	–	–	–	13	[38]
$Mo_{0.5}W_{0.5}S_2$	4.873	575	0.75	0.154	268	12	This work

and impurities, and nonlinear absorption. Therefore, in devices that implement mode-locked modulation, $Mo_{0.5}W_{0.5}S_2$ SA has a larger insertion loss. The mode-locked operation was unstable when the pump power exceeded 350mW.

Furthermore, in order to confirm that the mode-locking operation was achieved only by the $Mo_{0.5}W_{0.5}S_2$ SA, we replaced it by another uncoated FC/APC of the same size. In that case, the mode locking pulse could not be observed, even though the PC was adjusted carefully and the pump power was increased to maximum. The above experiment results confirm the $Mo_{0.5}W_{0.5}S_2$ SA can realized the effective mode-locking operations in the around 1.5 μm wavelength laser through the two-photon absorption. Therefore, the $Mo_{0.5}W_{0.5}S_2$ SA is able to played a significant role in the mode-locked operation.

In Table 1, we compared the $Mo_{0.5}W_{0.5}S_2$ SA with several novel nanomaterial-based SAs working around 1.5 μm. The result shows that $Mo_{0.5}W_{0.5}S_2$ films have a higher modulation depth, a higher peak power and the narrowest pulse compared with all other 12 TMDs SA-based lasers. A large single pulse energy of 25.57 nJ with a pulse width of 1.814 ns based on VSe_2/PVA was realized in Ref 30, corresponding to peak power of 1.849 W. The single pulse energy of 25.57 nJ was 166 times higher than that of our result. However, the corresponding pulse width of our result was fs level and the peak power of our result was 145 times larger than the work in Ref 30. The output power of 23.34mW with a pulse width of 709 fs was obtained based on the nonlinear optical modulation effect of NbS_2-microfiber SA. The pulse duration of 575 fs reported in our work was better than 709 fs. Notably, this was the first time mode-locking based on ternary $Mo_{0.5}W_{0.5}S_2$ SA. Thus, $Mo_{0.5}W_{0.5}S_2$ was a valuable material in short-pulse width laser generation.

5. Conclusion

In summary, the $Mo_{0.5}W_{0.5}S_2$/PVA was fabricated using microwave-assisted solvothermal method (MAST) and then sandwiched between two fiber end faces to serve as SA. Stable passively femtosecond mode locked EDFL with a tunable wavelength and a shorest pulse width of 575 fs was demonstrated using the ternary chalcogenide $Mo_{0.5}W_{0.5}S_2$ SA. These experimental results demonstrated that $Mo_{0.5}W_{0.5}S_2$ could be a potential candidate for femtosecond pulse fiber lasers. The $Mo_{(1-x)}W_xS_2$ alloys with different value of × will be investigated in our future work.

Declaration of Competing Interest

The authors declare that they have no known competing financial interests or personal relationships that could have appeared to influence the work reported in this paper.

Acknowledgments

This work was supported by the National Key R&D Program of China (No. 2018YFB1107200) and the National Natural Science Foundation of China (No. 61675158).

References

[1] U. Keller, Recent developments in compact ultrafast lasers, Nature 424 (6950) (2003) 831–838.
[2] F. Morin, F. Druon, M. Hanna, P. Georges, Microjoule femtosecond fiber laser at 1.6 μm for corneal surgery applications, Opt. Lett. 34 (13) (2009) 1991, https://doi.org/10.1364/OL.34.001991.
[3] M. Merker, R. Ackermann, R. Kammel, K.S. Kunert, S. Nolte, An in vitro study on focusing fs-laser pulses into ocular media for ophthalmic surgery, Lasers Surg. Med. 45 (9) (2013) 589–596.
[4] X. Han, Nanotube-Mode-Locked Fiber Laser Delivering Dispersion-Managed or Dissipative Solitons, J. Lightw. Technol. 32 (8) (2014) 1472–1476.
[5] A E J, S D, et al., 200fs mode-locked Erbium-doped fiber laser by using mechanically exfoliated MoS_2 saturable absorber onto D-shaped optical fiber, Opt. Express 25 (2017) 10546–10552.
[6] K. Wu, X. Zhang, J. Wang, et al., WS_2 as a saturable absorber for ultrafast photonic applications of mode-locked and Q-switched lasers, Opt. Express 3 (2015) 11453–11461.
[7] J. Yin, J. Li, H. Chen, et al., Large-area highly crystalline WSe_2 atomic layers for ultrafast pulsed lasers, Opt. Express 25 (2017) 30020–30031.
[8] Mengli Liu, Wenjun Liu, Zhiyi Wei, $MoTe_2$ Saturable Absorber with High Modulation Depth for Erbium-Doped Fiber Laser, J. Lightw. Technol. 37 (13) (2019) 3100–3105.
[9] Y.L. Wang, L.F. Li, et al., Monolayer PtSe2, a New Semiconducting Transition Metal Dichalcogenide, Epitaxially Grown by Direct Selenization of Pt, Nano Letters 15 (2015) 4013–4018.
[10] Yufeng Song, Si Chen, Qian Zhang, Lei Li, Luming Zhao, Han Zhang, Dingyuan Tang, "Vector soliton fiber laser passively mode locked by few layer black phosphorus-based optical saturable absorber,"*Opt*, Express 24 (23) (2016) 25933, https://doi.org/10.1364/OE.24.025933.
[11] L J, K J, et al. A femtosecond pulse erbium fiber laser incorporating a saturable absorber based on bulk-structured Bi2Te3 topological insulator, Opt. Express, 22, 6165-6173, (2014).
[12] X.T. Jiang, et al., Broadband nonlinear photonics in few-layer MXene Ti3C2Tx (T = F, O, or OH), Laser Photon. Rev. 12 (2018) 1700229.
[13] BF, et al. Graphene photonics and optoelectronics, Nature Pho., 4, 611, (2010).
[14] M, K F, L, et al. Atomically thin MoS2: A new direct-gap semiconductor," Phys. Rev. Lett. 105, 136805, (2010).
[15] C Y, et al. Tunable Band Gap Photoluminescence from Atomically Thin Transition-Metal Dichalcogenide Alloys, ACS Nano, 7, 4610-4616, (2013).
[16] Chenxi Dou, Wen Wen, Junli Wang, Mengyuan Ma, Liming Xie, Ching-Hwa Ho, Zhiyi Wei, Ternary $ReS_{2(1-x)}Se_{2x}$ alloy saturable absorber for passively Q-switched and mode-locked erbium-doped all-fiber lasers, Photon. Res. 7 (3) (2019) 283, https://doi.org/10.1364/PRJ.7.000283.
[17] Jie Li, Zilong Zhang, Lin Du, Lili Miao, Jun Yi, Bin Huang, Yanhong Zou, Chujun Zhao, Shuangchun Wen, Highly stable femtosecond pulse generation from a MXene $Ti_3C_2T_x$ (T = F, O, or OH) mode-locked fiber laser, Photon. Res. 7 (3) (2019) 260, https://doi.org/10.1364/PRJ.7.000260.
[18] M.Y. Ma, J. Zhang, Y. Zhang, et al., Ternary chalcogenide Ta2NiS5 nanosheets for broadband pulse generation in ultrafast fiber lasers, Nanophotonics 9 (2019) 2341–2349.
[19] Junli Wang, Lei Chen, Chenxi Dou, Haiting Yan, Lingjie Meng, Zhiyi Wei, $Mo_{0.5}W_{0.5}S_2$ for Q-switched pulse generation in ytterbium-doped fiber laser,

Nanotechnology 29 (22) (2018) 224002, https://doi.org/10.1088/1361-6528/aab5f2.
[20] H. Ahmad, et al., Mixed Transition Metal Dichalcogenide as Saturable Absorber in Ytterbium, Praseodymium, and Erbium Fiber Laser, IEEE Journal of Quantum Electronics (2018), https://doi.org/10.1109/JQE.2018.2822181.
[21] J.L. Wang, C. Dou, L. Chen, et al., High energy passively Q-switched Er-doped fiber laser based on $Mo_{0.5}W_{0.5}S_2$ saturable absorber, Opt. Mater. Express 8 (2018) 324–331.
[22] Y. Zhengyu, L. Tao, Z. Jia, et al., Generation of microsecond pulses at 1645 nm with $MoWS_2$ alloy, Optical Materials 84 (2018) 371–374.
[23] Hu Q., Wang J., Chen L., et al. Q-Switched Tm-doped fiber ring laser using Mo0.8W0.2S2 saturable absorber. CIOP100. doi: 10.1117/12.2505313.(2018).
[24] YuLin Min, Tao Wang, YouCun Chen, Microwave-assistant synthesis of ordered CuO micro-structures on Cu substrate, Applied Surface Science 257 (1) (2010) 132–137.
[25] Yung-Hsiang Lin, Sheng-Fong Lin, Yu-Chieh Chi, Chung-Lun Wu, Chih-Hsien Cheng, Wei-Hsuan Tseng, Jr-Hau He, Chih-I Wu, Chao-Kuei Lee, Gong-Ru Lin, Using n-and p-Type Bi_2Te_3 Topological Insulator Nanoparticles To Enable Controlled Femtosecond Mode-Locking of Fiber Lasers, ACS Photonics 2 (4) (2015) 481–490.
[26] G.-R. Lin, Y.-C. Lin, Directly exfoliated and imprinted graphite nano-particle saturable absorber for passive mode-locking erbium-doped fiber laser, Laser Physics Letters 8 (12) (2011) 880–886.
[27] Kangpeng Wang, Jun Wang, Jintai Fan, Mustafa Lotya, Arlene O'Neill, Daniel Fox, Yanyan Feng, Xiaoyan Zhang, Benxue Jiang, Quanzhong Zhao, Hongzhou Zhang, Jonathan N. Coleman, Long Zhang, Werner Josef Blau, Ultrafast Saturable Absorption of Two-Dimensional MoS_2 Nanosheets, ACS Nano 7 (10) (2013) 9260–9267.
[28] J.T. Wang, H. Chen, P.G. Yan, S.C. Ruan, Mode-locked thulium-doped fiber laser with chemical vapor deposited molybdenum ditelluride, Optics Letters 43 (9) (2018) 1998, https://doi.org/10.1364/OL.43.001998.
[29] H. Liu, A.P. Luo, et al., Femtosecond pulse erbium-doped fiber laser by a few-layer MoS_2 saturable absorber, Opt. Letters 39 (2014) 4591–4594.
[30] S J, S G, et al. Mode-locking in Er-doped fiber laser based on mechanically exfoliated Sb2Te3 saturable absorber, Opt. Mater. Express, 4, 1-6, (2014).
[31] M.H.M. Ahmed, et al., Mode-locking pulse generation with MoS_2-PVA saturable absorber in both anomalous and ultra-long normal dispersion regimes, Applied Optics 55 (2016) 4247–4252.
[32] Joonhoi Koo, Young In Jhon, June Park, Junsu Lee, Young Min Jhon, Ju Han Lee, Near-Infrared Saturable Absorption of Defective Bulk-Structured WTe_2 for Femtosecond Laser Mode-Locking, Advanced Functional Materials 26 (41) (2016) 7454–7461.
[33] D. Mao, X. She, B. Du, et al., Erbium-doped fiber laser passively mode locked with few-layer $WSe_2/MoSe_2$ nanosheets, Sci. Rep. 6 (2016) 23583.
[34] Jinho Lee, Yoontaek Kim, Kyungtaek Lee, Ju Han Lee, Femtosecond mode-locking of a fiber laser using a $CoSb_3$-skutterudite-based saturable absorber, Photon. Res. 6 (10) (2018) C36, https://doi.org/10.1364/PRJ.6.000C36.
[35] K. Ping, Y. Chun, et al., Passively Q-switched and femtosecond mode locked erbium-doped fiber laser based on a 2D palladium disulfide (PdS2) saturable absorber, Photon. Res. 8 (2020) 511–518.
[36] Li, Lu, et al. VSe2 nanosheets for ultrafast fiber lasers. Journal of Materials Chemistry C, 8,1104-1109,(2020).
[37] Yung-Hsiang Lin, Chun-Yu Yang, Sheng-Feng Lin, Wei-Hsuan Tseng, Qiaoliang Bao, Chih-I Wu, Gong-Ru Lin, Soliton compression of the erbium-doped fiber laser weakly started mode-locking by nanoscale p-type Bi_2Te_3 topological insulator particles, Laser Physics Letters 11 (5) (2014) 055107, https://doi.org/10.1088/1612-2011/11/5/055107.
[38] Yung-Hsiang Lin, Chun-Yu Yang, Jia-Hong Liou, Chin-Ping Yu, Gong-Ru Lin, Using graphene nano-particle embedded in photonic crystal fiber for evanescent wave mode-locking of fiber laser, Optics Express 21 (14) (2013) 16763, https://doi.org/10.1364/OE.21.016763.